permittivity" for the line is a function of the air and substrate permittivities and of the geometry of the line. Equation (6) clearly requires modification for this case. Qualitatively, however, since $(1/\epsilon)(\delta\epsilon/\delta T)$ for air is relatively small and negative an improvement in resonator temperature stability is expected. (From information in [6] it may be deduced that for air at 20°C and at constant pressure of 1 atm $(1/\epsilon)(\delta\epsilon/\delta T) = -1.8 \times 10^{-6}$/K.) The improvement, from 7 to 6 parts in 10^5/K as indicated in Table II, is fairly small since for microstrip most of the $\boldsymbol{E}$ field is still in the substrate.

The data in Table I may be used to predict the frequency coefficients for resonators on either orientation of sapphire, or our 96 percent alumina. For resonators on our alumina the frequency coefficients are about 10 percent lower than those indicated in Table II for sapphire, but as noted previously some variation is expected in the figures for alumina depending on the impurity content and the method of manufacture.

ACKNOWLEDGMENT

The authors wish to thank E. England for producing the substrate cavities, M. Matthews for assistance with the thermal expansion measurements, and C. Garrett for her work on the data analysis. Useful discussions with Dr. G. J. Gittens on the chemistry of alumina are also gratefully acknowledged.

REFERENCES

[1] P. H. Ladbrooke, M. H. N. Potok, and E. H. England, "Coupling errors in cavity-resonance measurements on MIC dielectrics," *IEEE Trans. Microwave Theory Tech.* (Short Papers), vol. MTT-21, pp. 560–562, Aug. 1973.

[2] F. Rosebury, *Handbook of Electron Tube and Vacuum Techniques.* Reading, Mass.: Addison-Wesley, 1965, p. 471.

[3] R. E. Collin, *Foundations for Microwave Engineering.* New York: McGraw-Hill, 1966, p. 353.

[4] W. George and P. Popper, "The dielectric properties of some commercial alumina materials at 9368 MHz," *Proc. Brit. Ceram. Soc.*, vol. 10, pp. 63–68, 1968.

[5] J. H. C. van Heuven and T. H. A. M. Vlek, "Anisotropy in alumina substrates for microstrip circuits," *IEEE Trans. Microwave Theory Tech.* (Short Papers), vol. MTT-20, pp. 775–777, Nov. 1972.

[6] R. C. Weast, Ed., *Handbook of Chemistry and Physics*, 50th ed., The Chemical Rubber Co., Cleveland, Ohio, 1970, Section E64.

Electromagnetic Power Absorption in Anisotropic Tissue Media

CURTIS C. JOHNSON, SENIOR MEMBER, IEEE,
CARL H. DURNEY, MEMBER, IEEE, AND
HABIB MASSOUDI, STUDENT MEMBER, IEEE

***Abstract*—Strong dielectric-constant anisotropy exists in muscle tissue at the lower microwave frequencies. Based on a model derived from tissue measurements, an analysis is carried out for single and multiple tissue layers. Calculated effects of tissue anisotropy on microwave fields and power absorption in the tissues are presented.**

Manuscript received July 19, 1974; revised November 11, 1974. This work was supported by the USAF School of Aerospace Medicine, Brooks Air Force Base, Texas.

C. C. Johnson is with the Department of Bioengineering, University of Utah, Salt Lake City, Utah 84112.

C. H. Durney and H. Massoudi are with the Departments of Bioengineering and Electrical Engineering, University of Utah, Salt Lake City, Utah 84112.

At frequencies below 100 Hz it is known that a strong conductance anisotropy exists in muscle tissue [1]. A fifteen-to-one difference in skeletal muscle resistivity has been measured at ECG frequencies. Schwan [2] attributes tissue permittivity and conductivity relaxation in the 1-MHz region to cell-wall polarization effects. This implies that relaxation effects exist when field components are normal to cell walls, but are not present with field components parallel to cell walls. In the work reported here, an idealized anisotropic tissue medium is assumed, consisting of infinitely long perfectly parallel muscle fibers generating relaxation effects only when there are E-field components perpendicular to the fibers. Based on this model, a theory is developed for field effects in anisotropic tissue, and equations for power absorption are derived.

Tissue data in the frequency range 0.001–100 MHz are based on data by Rush *et al.* [1], Schwan [2], and Johnson and Guy [3]. The data estimated from these references are summarized in Tables I and II for anisotropic skeletal muscle and fat.

Since the muscle medium consists of anisotropic conductivity and permittivity, a complex tensor permittivity is used

$$\bar{\epsilon} = \begin{vmatrix} \epsilon_x & 0 & 0 \\ 0 & \epsilon_y & 0 \\ 0 & 0 & \epsilon_z \end{vmatrix}.$$

The vector wave equation for the electric field in an anisotropic medium is derived from Maxwell's equations

$$\nabla^2 \boldsymbol{E} - \nabla(\nabla \cdot \boldsymbol{E}) + \omega^2 \mu_0 \bar{\epsilon} \cdot \boldsymbol{E} = 0.$$

When there are no transverse variations in the fields, as for plane-wave propagation in the z direction, the wave equation reduces to

$$(\partial^2 \boldsymbol{E}/\partial z^2) + \omega^2 \mu_0 \bar{\epsilon} \cdot \boldsymbol{E} = 0.$$

The solution to this second-order differential equation is

$$\boldsymbol{E} = E_x \hat{\boldsymbol{x}} \exp(-jk_x z) + E_y \hat{\boldsymbol{y}} \exp(-jk_y z)$$

TABLE I
ESTIMATED CONDUCTIVITY AND DIELECTRIC CONSTANT VARIATIONS IN SKELETAL MUSCLE IN THE y DIRECTION PERPENDICULAR TO THE MUSCLE FIBERS

f(MHz)	σ_y(mhos/m)	ϵ_y/ϵ_0
.001	.05	125,000
.01	.08	75,500
.1	.30	19,000
1.	.56	1,970
10.	.56	252
100.	.67	84.

Note: In the x direction, parallel to the fibers, we assume $\sigma_x = 0.67$ mho/m and $\epsilon_x/\epsilon_0 = 84$.

TABLE II
ESTIMATED CONDUCTIVITY AND DIELECTRIC CONSTANT VARIATIONS IN FAT

f(MHz)	σ_f(mhos/m)	ϵ_f/ϵ_0
.001	.028	50,000
.01	.031	20,000
.1	.033	4,000
1.	.036	314
10.	.038	30
100.	.040	7.5

where the propagation constants k_x,k_y are

$$k_x = \omega(\mu_0\epsilon_x)^{1/2} \qquad k_y = \omega(\mu_0\epsilon_y)^{1/2}.$$

With a knowledge of ϵ_x and ϵ_y from the tissue data in Tables I and II, we are now in a position to determine the field intensity and power absorption in an anisotropic tissue medium.

First, we consider a plane wave propagating in the $+z$ direction in an infinite anisotropic medium with the electric vector linearly polarized at $z = 0$ at an angle θ from the x axis. For this case the E_x and E_y fields become

$$E_x = E_0 \cos\theta \exp(-jk_x z) \qquad E_y = E_0 \sin\theta \exp(-jk_y z).$$

The time-averaged absorbed power density $\bar{P}_L$ in the medium is

$$\bar{P}_L = \tfrac{1}{2}\sigma_x E_x E_x^* + \tfrac{1}{2}\sigma_y E_y E_y^*.$$

The absorbed power density, at an arbitrary distance into the tissue $z = 1$ cm, as a function of polarization angle θ and frequency, is shown in Fig. 1. The muscle fibers are parallel to the x axis, and the electric field is parallel to the fibers at $\theta = 0°$. There is a striking difference in power absorption with the polarization angle at low frequencies due to the anisotropic conductivity. The absorbed power-density curves merge at higher frequencies because of reduced anisotropy.

We next consider a linearly polarized plane wave in air, striking a planar two-layer tissue model consisting of a fat layer of thickness d over anisotropic muscle. In order to solve for the electric-field distribution in the tissue layers, it is necessary to solve the boundary-value problem, matching the tangential electric and magnetic fields at the air–fat and fat–muscle interfaces $z = 0$ and $z = d$. The electric fields in the muscle tissue, $z > d$, become

$$E_x = \frac{2\cos\theta \exp[-jk_x(z-d)]}{[1 + (k_x/k_0)]\cos k_f d + j[(k_f/k_0) + (k_x/k_f)]\sin k_f d}$$

$$E_y = \frac{2\sin\theta \exp[-jk_y(z-d)]}{[1 + (k_y/k_0)]\cos k_f d + j[(k_f/k_0) + (k_y/k_f)]\sin k_f d}.$$

Corresponding expressions for power absorption in the fat and reflectance at the boundary $z = 0$ can also be obtained.

The magnitude of the reflectance R is shown in Fig. 2 for $\theta = 0°$ and 90°, for a fat thickness of 0.5 cm. In both cases, R is very high due to high tissue conductivity. For $\theta = 90°$, with current flow

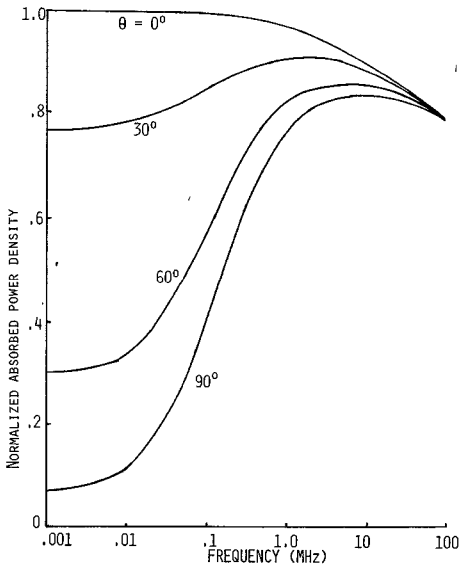

Fig. 1. Absorbed power density in an infinite anisotropic muscle medium as a function of polarization angle θ. The absorbed power density is calculated at $z = 1$ cm and normalized to the power density at $z = 0$ and $\theta = 0°$.

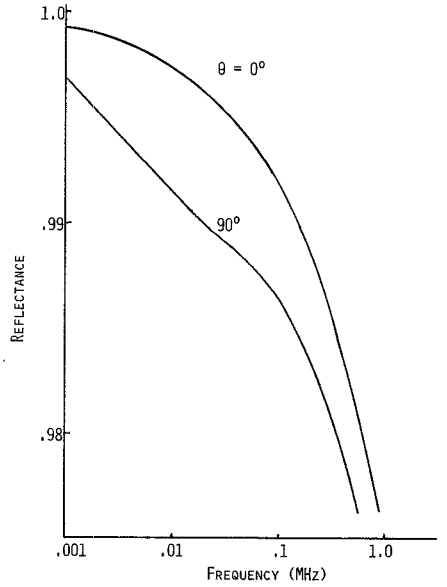

Fig. 2. Magnitude of the reflection coefficient in air for the planar two-layer model. Fat thickness is 0.5 cm. Incident plane-wave power density is 1 mW/cm^2.

across the muscle fibers, the reduced conductivity and higher dielectric constant cause a lower R value. Thus the field strength transmitted into the tissue is higher for $\theta = 90°$ than for $\theta = 0°$.

Absorbed power distributions within the tissue are shown in Figs. 3 and 4 for $f = 0.01$ MHz and $f = 1.0$ MHz, respectively. Fat power absorption is low because of lower conductivity. Power absorption in the muscle is remarkably insensitive to polarization angle at $f = 0.01$ MHz despite large conductivity and dielectric-constant differences. At $\theta = 0°$ the conductivity is much higher which would suggest more power absorption, but $|E|^2$ is lower because the higher conductivity has caused greater wave reflection. Fig. 5 shows the peak absorbed power density in the muscle at the fat–muscle interface as a function of frequency. Power absorption is slightly affected by the polarization at frequencies below 10 MHz, but not at higher frequencies.

A five-layer model is considered next, consisting of fat thickness equal to 1 cm, anisotropic muscle thickness equal to 7.5 cm, bone thickness equal to 3 cm, anisotropic muscle thickness equal to 7.5 cm, and fat thickness equal to 1 cm. This model is representative of the human leg. The properties of bone are assumed to be the same as those of fat. A transmission-line model is used to develop the equations for the electric and magnetic fields inside the various tissue layers. A transformation method is used to avoid the usual procedure of matching the boundary conditions and solving 12 simultaneous equations to find the field coefficients. The method uses Thevenin's theorem to transform the generator and its impedance to the right, and the usual impedance transformation is used to transform the load impedance to the left. Thus, to find the power absorbed in the third layer, the generator is transformed in two steps to the input of layer 3, and the load impedance is transformed in three steps to the output end of layer 3 to obtain the appropriate equivalent circuit. Although the expressions become complicated after more than one transformation, it is easy to write the general expressions and to program them on a computer, much easier than programming the computer to solve the 12 simultaneous equations which would be required in the usual solution of a boundary-value problem.

The results of these calculations for the five-layer model for two frequencies are shown in Figs. 6 and 7. Significant differences occur with polarization at $f = 0.01$ MHz, whereas, at $f = 100$ MHz, no differences are seen. Note that in the five-layer case for $f = 0.01$ MHz, the absorption in muscle for $\theta = 0°$ with greater σ is less than

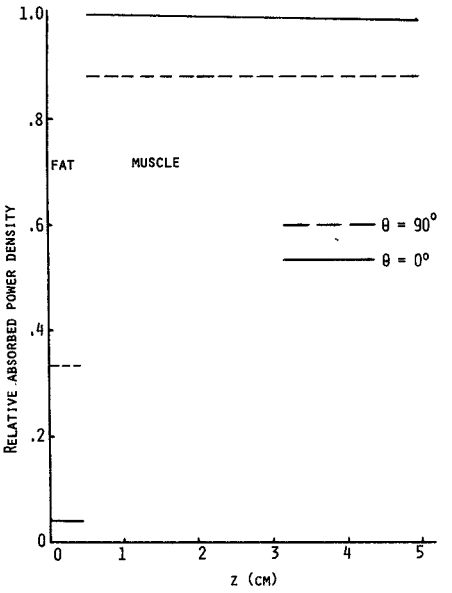

Fig. 3. Relative absorbed power density versus distance for the planar fat–muscle model; fat thickness is 0.5 cm, f = 0.01 MHz.

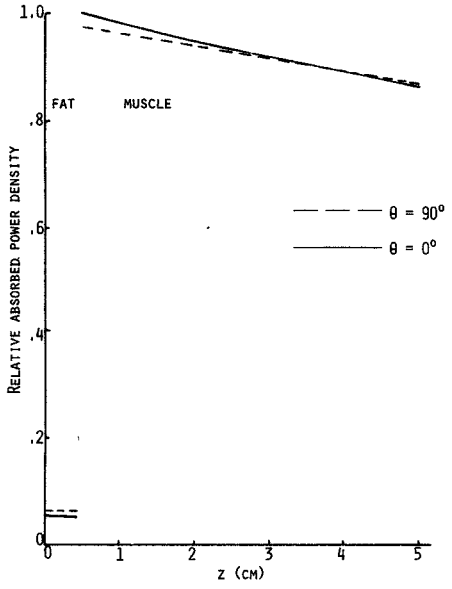

Fig. 4. Relative absorbed power density versus distance for the planar fat–muscle model; fat thickness is 0.5 cm, f = 1.0 MHz.

the absorption at $\theta = 90°$ with lower σ, a result opposite to that for the corresponding two-layer case of Fig. 3. This is probably caused by cumulative reflection-coefficient effects at the several tissue boundaries which differentially weaken the E field for $\theta = 0°$.

It should be emphasized that the model on which these calculations are based is limited because the infinite planar structure at these long wavelengths is not very representative of a human-sized or animal-sized body. The calculated data do indicate that, for this limited model, anisotropic effects can be significant at lower frequencies. The one-layer model predicts an over 10:1 difference in power absorption with polarization at 0.01 MHz and below. The two-layer model predicts a 12-percent difference in power absorp-

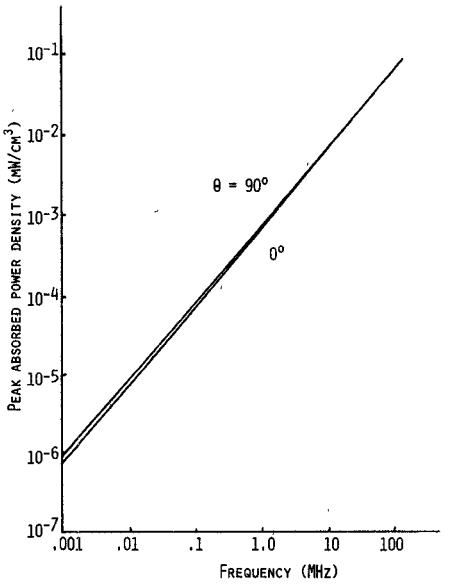

Fig. 5. Peak absorbed power density versus frequency for the planar fat–muscle model. Fat thickness is 0.5 cm. Incident plane-wave power density is 1 mW/cm².

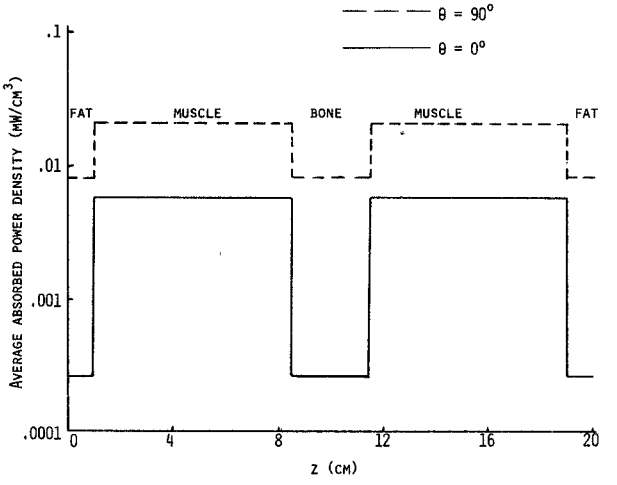

Fig. 6. Absorbed power density versus distance for the five-layer model. Incident plane-wave power density is 1 mW/cm², f = 0.01 MHz.

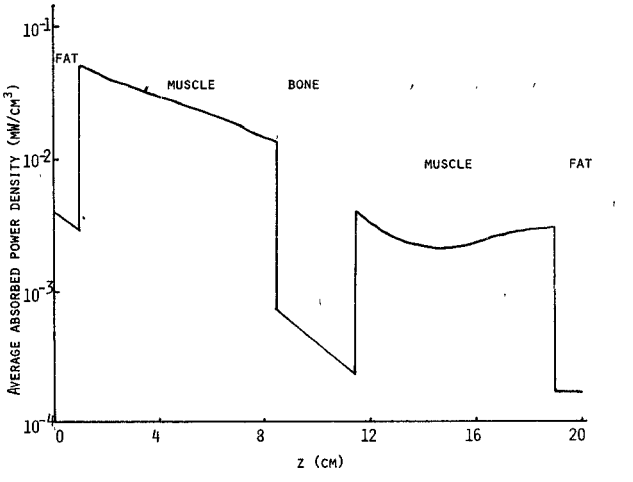

Fig. 7. Absorbed power density versus distance for the five-layer model for both $\theta = 0°$ and $\theta = 90°$. Incident plane-wave power density is 1 mW/cm², f = 100 MHz.

tion with polarization at 0.01 MHz. The five-layer model predicts about a 5:1 difference.

In conclusion, it is predicted theoretically that marked differences in tissue-absorbed power density can occur due to tissue anisotropy at frequencies below 10 MHz. Further research efforts on anisotropic effects must include more appropriate models. Whereas the model assumes infinitely long one-directional muscle fibers, actual skeletal muscle tissue contains finite fiber lengths. This is of little consequence in the model. In the legs and arms, muscle-fiber orientation is reasonably uniform and the one-directional model is useful. However, in other portions of the body skeletal muscle fibers are layered and run in several different directions. The model must be refined in these areas of the body. A finite-layered model such as an anisotropic sphere or spheroid is needed to extend the infinite-layered model results. The finite-model analysis is required before useful predictive quantitative data can be obtained. It has been previously demonstrated in this frequency range that body orientation with respect to the RF field vectors is an important factor in tissue-absorbed power density [4]. It is expected that body orientation combined with anisotropic effects will play a major role in effecting absorbed RF power density.

REFERENCES

[1] S. Rush, J. A. Abildskov, and R. McFee, "Resistivity of body tissues at low frequencies," *Circ. Res.*, vol. 12, pp. 40–50, Jan. 1963.
[2] H. P. Schwan, "Electrical properties of tissue and cell expansions," *Biol. Med. Phys.*, vol. 5, pp. 147–209, 1957.
[3] C. C. Johnson and A. W. Guy, "Nonionizing electromagnetic wave effects in biological materials and systems," *Proc. IEEE*, vol. 60, pp. 692–718, June 1972.
[4] C. H. Durney, C. C. Johnson, and H. Massoudi, "Long wavelength analysis of planewave electromagnetic power absorption by a prolate spheroidal tissue body," in *Proc. 1974 Annu. USNC-URSI Meeting* (Boulder, Colo., Oct. 1974), p. 110.

Fiber and Diffused Waveguide Structures for Distributed-Feedback Lasers

C. ELACHI, MEMBER, IEEE,
G. EVANS, STUDENT MEMBER, IEEE, AND
C. YEH, MEMBER, IEEE

***Abstract*—Optimum threshold conditions for oscillations of transversely bounded distributed-feedback (DFB) lasers are derived and discussed for the case of a fiber guide and diffused guide.**

The recent development of integrated-optics thin-film distributed-feedback (DFB) lasers [1]–[9] has generated much interest in the application of the DFB concept to other types of lasers. Basically, the DFB approach consists of replacing the two end mirrors by a volume or surface Bragg grating, throughout the active medium, which would provide enough feedback for self-sustained oscillation. Kogelnik and Shank [4] have analyzed in detail the properties of transversely unbounded DFB lasers. Elachi and Yeh [10] and Elachi *et al.* [11], have studied the case of a thin-film DFB laser and have shown that the presence of the transverse boundary has drastic effects on the feedback coupling and threshold gain. In this short paper, we derive the threshold conditions for fiber and diffuse DFB lasers, and we show that these structures are feasible with available active materials. A fiber DFB laser [Fig. 1(a)] can be used as a source of an optical-fiber communication channel and thus eliminate the input-coupling problem. A diffused-guide DFB laser [Fig. 1(d)] is attractive because it is easy to implement [12]. A gas-capillary laser with diffused cladding [Fig. 1(c)] has the advantage that it can support guided waves [13]. A diffuse guide has recently been developed [12] and analyzed [14]. Homogeneous-capillary DFB lasers were proposed by Marcuse [7].

If the boundary of an active waveguide is corrugated with a perturbation $\eta \cos(2\pi z/\Lambda)$, two contradirectional modes (p and q) are strongly coupled if they satisfy the Bragg condition

$$\beta_p + \beta_q = 2\pi/\Lambda \tag{1}$$

where β_i are the longitudinal wave vectors.

The coupling coefficient κ_{pq} [1], [15], [16], can be derived, in the case of small surface perturbation, by replacing the surface corrugation with a periodic surface current [11], [15], or by solving the exact boundary condition [10]. We found the coupling coefficient to be equal to

$$\kappa_{pq} = \eta \frac{\epsilon_1 - \epsilon_2}{2} k^2 (Q_p Q_q)^{-1/2} \tag{2}$$

where $k = \omega/c$ and Q_i are given in Table I for the fiber and diffuse guide case, and η is the amplitude of the periodic surface perturbation.

If one of the regions (inside or outside the guide) is an active medium with gain coefficient G, the effective gain coefficient would then be CG. This is due to the fact that the optical energy is never totally confined to the active region. The value of C was determined by taking the dielectric constant to be complex in the gain region and then solving for the (complex) longitudinal wave vector β_i. For small gain, a Taylor expansion series gives

$$C_i = \frac{k(\epsilon_1)^{1/2}}{\mathrm{Re}\{\beta_i\}} \frac{F_i}{1 + F_i} \tag{3}$$

for the case where the guiding region is active (inside the fiber or in the inhomogeneous half-space), and

$$C_i = \frac{k(\epsilon_2)^{1/2}}{\mathrm{Re}\{\beta_i\}} \frac{1}{1 + F_i} \tag{4}$$

for the case where the outside region is active (cladding or homogeneous half-space). The expression F is given in Table I. Independently, it can be shown that in the case of an active fiber the coefficient C_i is equal to

$$C_i = \frac{k(\epsilon_1)^{1/2}}{\mathrm{Re}\{\beta_i\}} \frac{P}{P + P'} \tag{5}$$

where P and P' are the powers inside and outside the fiber. The first term in (5) expresses the fact that the optical ray follows a zigzag line.

The threshold gain can now be determined by using a modified form [11] of the Kogelnik and Shank approach [4] to take into account the fact that the forward and backward waves could be different modes, and therefore might have different effective gains and group velocities.

The required threshold gain for laser oscillation is given by

$$G = \frac{2}{C_p(k) + C_q(k)} \mathrm{Re}\{Y_{pq}\} \tag{6}$$

and the corresponding phase mismatch by

$$\Delta k = \frac{2}{c(\psi_p(k) + \psi_q(k))} \mathrm{Im}\{Y_{pq}\} \tag{7}$$

where Y_{pq} is a solution of

Manuscript received May 6, 1974; revised January 17, 1975. This work was supported in part by NASA Contract NAS7-100, and in part by the Naval Electronics Laboratory Center.

C. Elachi and G. Evans are with the Jet Propulsion Laboratory, California Institute of Technology, Pasadena, Calif. 91103.
C. Yeh is with the Department of Engineering, University of California, Los Angeles, Calif. 90024.